Journal of Cleaner Production 292 (2021) 126108

Contents lists available at ScienceDirect

Journal of Cleaner Production

journal homepage: www.elsevier.com/locate/jclepro

The degradation of di-(2-ethylhexyl) phthalate, DEHP, in sediments using percarbonate activated by seaweed biochars and its effects on the benthic microbial community

Chang-Mao Hung [a], Chin-Pao Huang [b], Chiu-Wen Chen [a], Cheng-Di Dong [a, *]

[a] Department of Marine Environmental Engineering, National Kaohsiung University of Science and Technology, Kaohsiung City, Taiwan
[b] Department of Civil and Environmental Engineering, University of Delaware, Newark, USA

ARTICLE INFO

Article history:
Received 1 September 2020
Received in revised form
3 January 2021
Accepted 22 January 2021
Available online 26 January 2021

Handling Editor. M.T. Moreira

Keywords:
Biochar
Estuarine sediments
Microbial communities
Phthalates

ABSTRACT

Di-(2-ethylhexyl) phthalate (DEHP) is a highly toxic and persistent contaminant. Elimination of DEHP from the environment is crucial to safe guard ecological and human health. Red seaweed-derived biochar (RSB), made from *Agardhiella subulata* residues, was used to activate sodium percarbonate (SPC) for the degradation of DEHP in contaminated estuarine surface sediments. The RSB was characterized by scanning transmission electron microscope-energy dispersive X-ray spectroscopy (STEM-EDS), micro-attenuated total reflectance-Fourier transform infrared spectroscopy (MATR-FTIR), elemental analysis (EA), thermogravimetric analysis (TGA), X-ray photoelectron spectrometry (XPS), linear sweep voltammetry (LSV), and Tafel measurements. Results revealed that the increase in SPC dosage, specifically, [DEHP] to [SPC] molar ratio of 1:1000, increased DEHP removal in the sediment. The pyrolysis temperature (300–900 °C) for biochar preparation significantly controlled the particle size and catalytic capacity of RSB. Pristine RSB contributed catalytic sites, which effectively activated SPC via electron transfer through the RSB matrix, that generated HO• and facilitated the carbocatalysis degradation of DEHP. RSB900 was the best-performing SPC activator. Under the optimal initial pH of 9, total DEHP degradation was 63% in 12 h. Treatment with RSB and SPC, significantly increased the bacterial abundance in the sediment. Results of next-generation sequencing analyses showed that *Proteobacteria* and *Bacterioidetes* were the dominant bacterial phyla. The microbial abundance and diversity of the sediment ecosystems were improved significantly upon treatment by the RSB–SPC process, indicating the efficacy of the remediation technology. Results provide valuable insights into the role of microbial communities as indicators of sediment quality.

1. Introduction

Gao and Wen (2016) have reported that phthalate esters (PAEs), plasticizers of plastics or polymeric materials, are detected frequently in both fresh water and sediments. Chen et al. (2017) and Zhang et al. (2018) have cautioned the potential environmental and health risks of PAEs contamination of ecosystems. Many sediment-bound contaminants, such as di-(2-ethylhexyl) phthalate (DEHP), are refractory endocrine disrupting compounds (EDCs) that impose great risks to aquatic ecosystems because of ubiquitous nature, resistant to microbial degradation, low water solubility, and long hydrocarbon chains (Mi et al., 2019; Zhu et al., 2020). Urbanization and industrialization have brought widespread distribution of DEHP in the environment. DEHP elevated concentration in numerous aquatic and terrestrial environments (e.g., lakes, lagoons, rivers, wetlands, streams, soil, sludge, and sediments) associated with its carcinogenic effects and environmental persistence are great threats to environmental and human health (Zhao et al., 2016; Hu et al., 2020). The U.S. Environmental Protection Agency has classified DEHP an EDC (USEPA, 2007). Therefore, there are urgent needs to eliminate DEHP from the environment for minimizing its deleterious impacts on ecosystems and human. Presently, technologies such as microbial biodegradation and advanced oxidation processes (AOPs) have been attempted (Xu et al., 2017; Dong et al., 2019a, b; Annamalai and Vasudevan, 2020). Specifically, an integrated chemical-biological method for *in-situ* or *ex-situ* treatment

* Corresponding author.
E-mail address: cddong@nkust.edu.tw (C.-D. Dong).

https://doi.org/10.1016/j.jclepro.2021.126108
0959-6526/

of DEHP-contaminated sediments could be a promising remediation strategy (Chen et al., 2009; Dong et al., 2020a; Xie et al., 2020).

Percarbonate-based advanced oxidation processes are cost-competitive, efficient, and environmentally sustainable for the remediation of impaired surface and subsurface waters and soils (Ma et al., 2018). Recently, Zuo et al. (2020) have studied the removal of electron-rich recalcitrant organic contaminants using solid sodium percarbonate ($2Na_2CO_3 \cdot 3H_2O_2$, SPC). Gao et al. (2020a) investigated the removal of bisphenol A (BPA) from wastewater by ultraviolet light activation of SPC (UV/SPC) and reported that both HO• ($E^0 = 2.32$ V vs. standard hydrogen electrode (SHE) at pH 7) and $CO_3^{-\bullet}$ ($E^0 = 1.78$ V vs. SHE at pH 7) causing BPA degradation.

Lyu et al. (2020) investigated the removal of trichloroethylene (TCE) from groundwater using SPC activated by Fe(II)-citrate complex and reported that the Fe(III)/Fe(II) redox couple that enhanced the production of HO•/$O_2^{-\bullet}$ radicals for almost complete TCE removal. Li et al. (2020a, b) reported that Fe(II) activation of SPC significantly improved sludge dewaterability and humic acid degradation. Ren et al. (2020) demonstrated that Fe(II)-SPC pretreatment of algae-laden UF membrane minimized fouling. Above recent studies indicated that Fe^{2+} was effective in SPC activation for enhancing the degradation of organic contaminants. However, the soluble metal ions can bring about secondary pollution problems, thereby limiting the engineering deployment, especially in *in-situ* applications (J. Yu et al., 2020). Therefore, there are needs of environmentally friendly and low cost biomass-based metal-free materials such as biochar as SPC activators for *in-situ* remediation of contaminated sediments (Hung et al., 2021).

A wide variety of waste biomass have been used to make biochar via thermochemical conversion process (e.g. pyrolysis) under limited oxygen condition (Lam et al., 2017; Liew et al., 2018). Pyrolysis temperature and the type of feedstock were found to greatly influence the physiochemical properties of biochar, including specific surface area, porosity, surface functional groups, elemental contents, and pH value (Yek et al., 2020). Therefore, it is challenging to select appropriate pyrolysis conditions and feedstock in preparing biochars for specific applications. Biochar for carbocatalytic AOP application as a framework of circular bioeconomy has received increasingly attention recently (Wang and Wang, 2020). Hung et al. (2020a, b) have recently studied the removal of organic contaminants using carbocatalysis SPC in the presence of carbonaceous materials such as seaweed- and sludge-derived biochar. Chen et al. (2020) reported the preparation of biochar from anaerobic digestion sludge, an environmentally friendly material, as peroxydisulfate (PDS) activators. Wan et al. (2020) demonstrated the carbocatalytic degradation of BPA on a tartaric acid-treated iron-impregnated biochar (Fe–CBC–TA) prepared from cellulosic biomass in a peroxymonosulfate (PMS) activation system. Nie et al. (2019) illustrated that polarized carbocatalyst (i.e., multi-walled carbon nanotubes, MWCNTs) catalyzed-peroxydisulfate (PDS) activation in an electrosorption system effectively removed acyclovir and phenol in aqueous solutions.

Intuitively, while oxidation treatment may reduce the DEHP level in contaminated environments, the intrinsically strong oxidation capability of the process can also negatively impact the indigenous microbial communities in treated soil/sediment ecosystems (Gou et al., 2020). Therefore, microbial diversity plays crucial roles in sustaining the ecological functions and stability of aquatic ecosystems. To date, there is little information on the effects of biochar-activated SPC carbocatalysis on the biological responses of sediment.

In the present study, we developed a facile method to synthesize red seaweed-derived biochar (RSB) as SPC activator for the remediation of PAEs-contaminated sediments exemplified by DEHP. As far as we know there was no investigation on the removal of DEHP from estuarine sediments by combined RSB and SPC treatment. Biochar preparation condition, specifically, pyrolysis temperature, affecting the SPC activation capacity of RSB was investigated. Several parameters, such as SPC and RSB dosage, and pH on DEHP removal were studied. Finally, the dynamics of microorganism consortium in the RSB–SPC treated sediments were examined systematically by high-throughput next-generation sequencing (NGS) techniques.

2. Materials and methods

2.1. Sampling and characterization of sediments

Sediment samples were collected from an estuary section of the Jen-Gen River in Kaohsiung, Taiwan (120°17.92′ E in longitude and 22°35.06′ N in latitude) with an Ekman Dredge grab sampler. The samples immediately after dredging were placed in amber glass bottles, pre-cleaned with *n*-hexane and Teflon-lined cap sealed. The glass bottles were kept in an icebox while transporting back to laboratory. Then, the samples were dried in the air under ambient temperature for 7 days before freeze-drying in a vacuum freezing dryer (FD-5030/8530, Panchum Scientific Co. Ltd., Taiwan) for 72 h. Results of textural analysis of the natural sediment sample showed 24, 68, and 8% of sand, silt, and clay, respectively, which represented typical silt-loam structure.

2.2. Chemicals

Sodium percarbonate ($2Na_2CO_3 \cdot 3H_2O_2$, SPC) (20–30% H_2O_2) was purchased from Sigma-Aldrich Co. Ltd. (St. Louis, MO, USA). Acetone (99.8% purity, HPLC grade), methanol (99.8% purity, HPLC grade), and *n*-hexane (99.8% purity, HPLC grade) were acquired from Echo Chemical Co. Ltd. (Kaohsiung, Taiwan). Di-(2-ethylhexyl) phthalate ($C_{24}H_{38}O_4$, DEHP) and branched side-chain-mixed compounds (99.5% purity) were bought from Tokyo Kasei Kogyo Co. Ltd. (Chuo City, Tokyo, Japan). Internal standard (p-terphenyl, 99.5% purity) was procured from Chem Service Inc. (West Chester, PA, USA). N, N-dimethylformamide (DMF) was bought from J.T. Baker (Radnor, PA, USA). All of the above chemicals used were of analytical grade.

The biochar was made from red seaweed (*Agardhiella subulata*) residue by pyrolysis as previously reported (Hung et al., 2020a). Briefly, the collected pristine red seaweed extract residues were first washed thoroughly under running water to remove external impurities; then, the algal residues were dried in air for 24 h followed by drying at 60 °C for 1 day in an oven till complete dryness. Finally, the dried seaweed biomass was ground into powder using pestle and mortar. The powdered material, in ceramic boat, was put in a tube furnace and heated under flowing CO_2 gas at the desired temperature (300–900 °C) and ramping rate of 10 °C min^{-1} for 2 h to produce the RSB. After cooled to room temperature, the samples were removed and then thoroughly ground again. The RSB samples were labeled as RSBX, where X represented the pyrolysis temperature, namely, 300, 500, 700, and 900 °C, individually.

2.3. DEHP degradation experiments

A series of DEHP degradation experiments were carried out in 40-mL borosilicate glass tubes (capped with PTFE cover) containing 1 g of dry sediment sample at room temperature (30 °C). The catalytic oxidation reaction was initiated by adding a certain amount of RSB (0.015–0.075 g) to 25 mL of solution containing SPC and DEHP at molar ratio in the range of 1:1 to 1000:1 in 40-mL borosilicate glass tubes. After being shaken gently for 30 s in a water

bath shaker (SB-9D, Taiwan Hipoint Corporation, Kaohsiung, Taiwan) the vials were continuously shaken at 200 rpm for 12 h. At specific time interval, the 1 g of sediment sample was withdrawn and immediately added 1 mL of methanol to quench the reaction. Extracted the sediment slurry with 5 mL acetone/n-hexane (1:1) to analyze the residual DEHP concentration for determining the percentage of DEHP removal. The concentration of DEHP was determined by gas chromatograph−mass spectrometry (GC−MS), Agilent model 6890 gas chromatograph equipped with Agilent 5975 mass selective detector and HP-5MS (30 m × 0.25 mm i.d. × 0.25 μm film thickness) (Hewlett-Packard, Palo Alto, CA, USA) operated in selective ion monitoring (SIM) mode. Dong et al. (2020a) have reported the detailed procedure for the analysis of DEHP previously. The initial pH was adjusted with HCl (0.1 M) and/or NaOH (0.1 M) for studying the effect of pH on DEHP degradation by the RSB/SPC system. The effect of RSB dosage on DEHP degradation was investigated also. All DEHP degradation experiments were run in triplicates with mean value being reported.

2.4. Characterization of biochar

An STEM system equipped with an EDS attachment (JEM-3010, JEOL, Tokyo, Japan) was used for microstructural with elemental composition analysis of RSB. The MATR-FTIR spectrum was recorded on an ATR-FTIR spectrometer connected to an optical microscopy (Nicolet iN10, Thermo Fisher Scientific, Waltham, MA, USA) for confirming the presence of various functional groups of biochar. The C, H, and O content was determined with elemental analyzer (Vario EL III, Hanau, Germany). The thermogravimetric (TGA) property was performed as well by using TGA instrument (TA Q500, TA Instruments, Wilmington, DE, USA). The temperature was increased from room to 1000 °C at 10 °C min^{-1} of ramping rate in pure nitrogen atmosphere. The surface chemical structure and composition were studied using X-ray photoelectron spectroscopy (XPS, AXIS Ultra DLD, Kratos Analytical Ltd., Manchester, UK). The polycyclic aromatic hydrocarbon (PAH) content of RSB was analyzed using GC−MS (Model 6890/5975, Agilent Technologies, Santa Clara, CA, USA). The analytical condition for PAHs followed that previously reported in details by Dong et al. (2017, 2018, 2020b). Linear sweep voltammetry (LSV) and Tafel polarization curve were obtained with an electrochemical workstation (CHI 6081D, USA) (Hung et al., 2020c). The RSB in Na_2SO_4 (0.5 M) electrolyte was scanned in the potential range between −2.0 and 2.0 V versus Ag/AgCl electrode at 25 mV s^{-1}. A glassy carbon electrode (GCE) (75 mm × 6 mm o.d. × 3 mm i.d) (model CHI104, CH Instruments, Inc. Austin, TX, USA) and platinum wire (10 mm × 0.5 mm o.d.) were used as the working and the counter electrode, respectively. The working electrode was prepared by dispersing 1 mg of RSB in 1 mL of DMF to give a homogeneous suspension in a sonic bath, then 5 μL of the suspension were drop-coated onto the GCE surface followed by air-dried at room temperature. Electron paramagnetic resonance spectroscopy (EPR; EMXnano, Bruker, Germany) with DMPO (0.1 M) as a spin-trapping agent was used to qualify and quantify the production HO• radicals, which concentration was determined, after correcting for background-noise intensity of DMPO-HO• peaks (Hung et al., 2020d).

2.5. Assessment of bacterial community

For the assess change in microbial community structure following RSB-SPC treatment, the genomic DNA in the sediment sample was extracted by using QIAamp® PowerFecal® DNA Kit (Qiagen, Hilden, Germany). The following four sediment treatment systems were assessed: (a) control without RSB and SPC, (b) with SPC, (c) with RSB, and (d) with both RSB and SPC. The microbial community of the treated sediments were studied with the Illumina MiSeq platform (Illumina Miseq PE250, San Diego, CA, USA) supported by BIOTOOLS Co., Ltd. (Taipei, Taiwan). The V3−V4 region of the 16S rRNA gene was amplified by using polymerase chain reaction (PCR) with universal primers 319F (5′-CCTACGGGNGGCWGCAG-3′) and 806R (5′-GACTACHVGGGTATCTAATCC-3′) according to the 16S Metagenomic Sequencing Library Preparation procedure (Illumina, San Diego, CA, USA). The samples were further subjected to a QIIME-based microbiota analysis. Conditions for PCR analysis were: first, denaturation at 95 °C for 3 min, second, 25 cycles each at 95 °C for 30 s, 55 °C for 30 s, 72 °C for 30 s, and 72 °C for 5 min, and finally, at 4 °C for 1 cycle. The PCR products were analyzed by electrophoresis on 1.5% agarose gel (Sigma-Aldrich, Poole, UK). Samples with a bright main strip around 500 bp were chosen and purified with AMPure XP beads (Beckman Coulter) according to the manufacturer's protocol. An equal amount of the indexed PCR product was mixed to generate the sequencing library. Last, the library was sequenced on an Illumina MiSeq 2500 platform (Illumina, San Diego, USA), and 300 bp paired-end reads were generated based on a threshold of 97% similarity; operational taxonomic units (OTUs) were clustered by using UPARSE (version 7.1), and taxonomic classifications were assigned according to the information retrieved from the Greengenes database (version 13.8). The community diversity indices i.e., Simpson and Shannon and richness indices (Chao 1 and Abundance-based Coverage Estimator (ACE)) were calculated by using MOTHUR v.1.30.1 software. Venn diagrams were constructed with the gplots package in R software v. 2.10.1, to compare shared and unique species among different treatments. An hierarchical clustering analysis was performed by using Primer 6 software.

3. Results and discussion

3.1. Characterization of the red seaweed-based biochar (RSB)

Fig. 1a and b represents the STEM images of RSB samples, RSB300 and RSB500. Results showed irregular agglomerates with overlapped structures when severe coalescence occurred on RSB during pyrolysis of seaweed biomass. The aggregates, which collected a group of nanoparticles were in the size range of 50−100 nm (Fig. 1a and b). Results of EDS analysis confirmed the presence of C, O, and Ca on the RSB surface. The RSB700 sample exhibited a spindle-like and dense structure of spherules aggregates (Fig. 1c). The RSB900 sample showed uniform spherical shape particles with a diameter of ~30 nm (Fig. 1d). With increasing temperature, the particle size and the content of C decreased, while Ca content of the biochar increased, because of increase in the condensation of mineral compositions (e.g. Ca) in the biochar with increasing pyrolysis temperature during thermochemical conversion process (Yang et al., 2015). The results suggested that pyrolysis successfully incorporated calcium materials in the biochar matrix; a similar phenomenon was observed in previous study (Hung et al., 2020a).

Fig. 1e-l gives results of MATR-FTIR image and spectra for RSB at different pyrolysis temperatures, obtained in the wavenumber region from 400 to 4000 cm^{-1}. Micro images of the RSB showed spherically structured agglomerates with diameters less than 50 μm in different RSB samples (Fig. 1e−h). The band around 689, 900, and 1430 cm^{-1}, respectively, represented the asymmetric stretch mode of Ca−O bond (Wang et al., 2019). It is worth noting that the increase in band intensity of Ca−O, observed on RSB900, provided information on the surface functionalization process. Moreover, three peaks were observed at 3435, 2926, 1160, and 1030 cm^{-1} corresponding to the stretching vibration of O−H in the

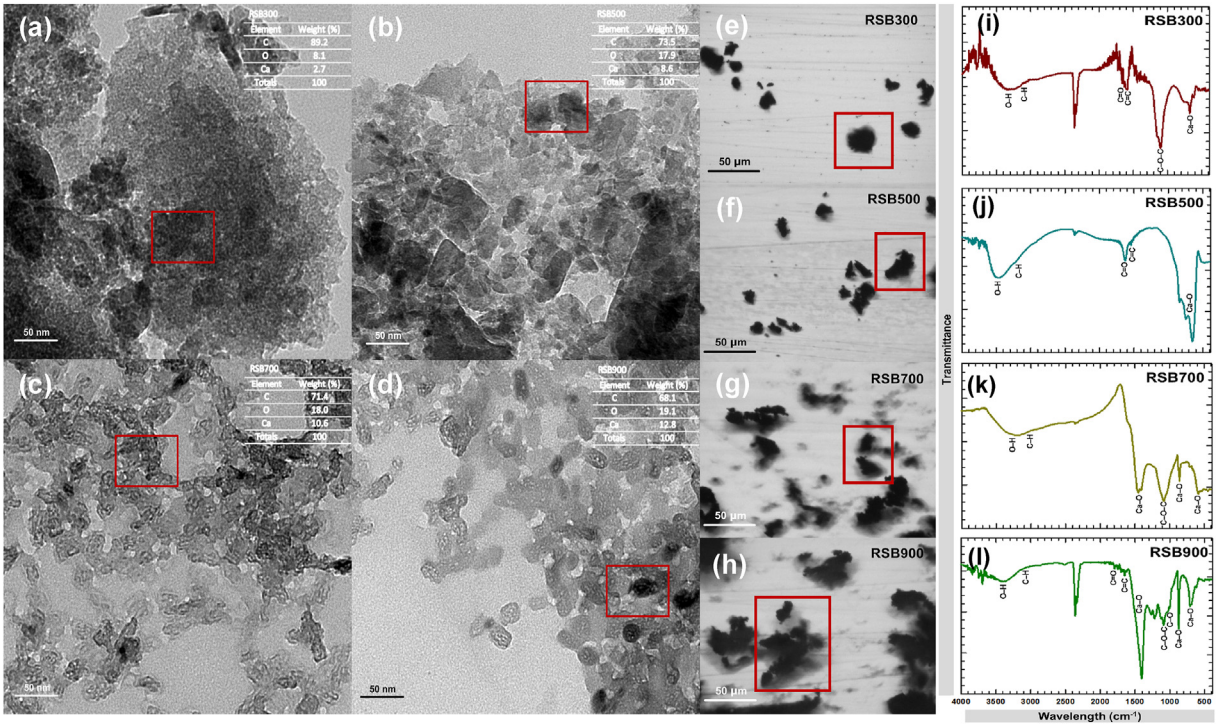

Fig. 1. The (a–d) STEM and (e–l) MATR-FTIR spectra of RSB catalyst. RSB300 (a, e, i); RSB500 (b, f, j); RSB 700 (c, g, k); RSB900 (d, h, l). The red-line box shows the correspondingly selected observation area.

plane of free hydroxyl groups, the aliphatic sp^3 hybridized C–H stretching vibrations, surface C–O–C, and C–O bonds stretching vibrations associated with carbohydrate structures, respectively. Some bands due to aromatic C=C and carbonyl C=O bonds stretching vibrations in the region 1500–1800 cm^{-1} suggested the formation of aromatic structures during pyrolysis of the RSB (Zubkova et al., 2019).

The O/C and H/C molar ratio of the RSB were plotted in form of Van Krevelen diagram (Fig. 2a). The development of functional aromatic groups via the removal of hydrogen and oxygen atoms from raw biomass resulted in a decrease in the H/C and O/C atomic ratio, from 0.04 to 0.01 and 0.5 to 0.1, respectively, which confirmed the loss of carboxyl groups through decarboxylation and increase in aromaticity and hydrophobicity of biochars resulted from pyrolysis

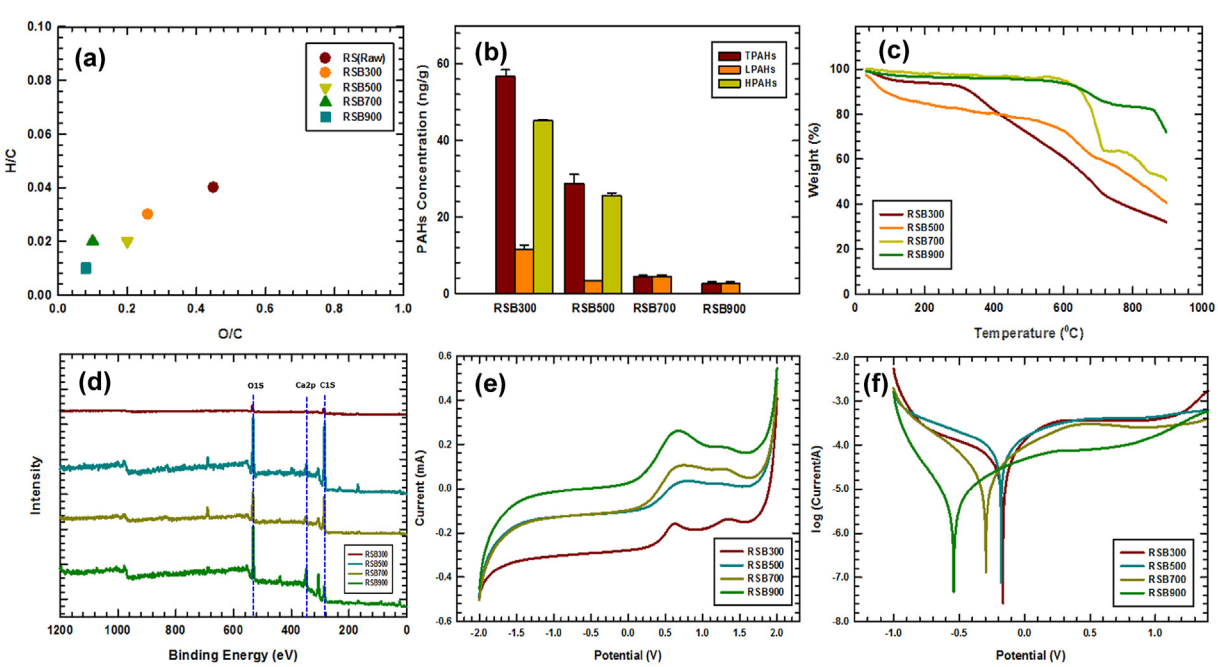

Fig. 2. The (a) Van Krevelen plot, (b) content of PAHs, (c) TGA, (d) XPS, (e) LSV, (f) Tafel spectra of RSB catalyst.

temperature (De Bhowmick et al., 2018; Azargohar et al., 2019).

Generally, PAH concentration remained high in the temperature range of 300–500 °C then decreased abruptly at temperature greater than 700 °C. Total PAHs (TPAHs) level followed the order: RSB300 > RSB500 > RSB700 > RSB900 (Fig. 2b). RSB300 had the highest level in both high-molecular-weight PAHs (HPAHs, four-to six–rings) and low-molecular-weight PAHs (LPAHs, two-to three-ring) fractions. However, both HPAHs and LPAHs levels deceased in biochar as the pyrolysis temperature increased. Notably, the PAHs disappeared in RSB700 and RSB900.

Fig. 2c gives the TGA curve of RSB samples. The weight of RSB300 and RSB500 decreased steadily from 25 °C until 700 °C. Results showed a weight loss at 110 °C due to loss of physically adsorbed moisture. The weight loss between 150 and 300 °C was correspondent to the decomposition of hemicellulose components (Lam et al., 2017). The weight loss between 300 and 700 °C was due to the combustion of cellulose, lipids and lignin components of seaweed (De Bhowmick et al., 2018; K.L. Yu et al., 2020). Furthermore, the TGA curve of RSB900 showed relatively high thermal stability in the initial decomposition temperature range from 25 to 700 °C. Increase in pyrolysis temperature from 700 to 800 °C exhibited further weight drop, followed by a less obvious weight loss at temperature between 800 and 900 °C. The above weight changes were related to the development of aromatic structure in biochars and/or the decomposition of inorganic residues on the surface of RSB (Azargohar et al., 2019).

The XPS survey scan spectrum showed that all RSB samples were mainly related to three elements, i.e., C1s, Ca2p, and O1s (Fig. 2d). The peak at 284.7, 347.2, and 531.7 eV represented the binding energy of carbon, calcium, and oxygen, respectively. The reaction between CaO and biochar that decreased carbon content in biochar matrix was observed by XRD and reported previously (Hung et al., 2020a) (Fig. S1). As the pyrolysis temperature increased from 300 to 900 °C, the peak intensity of Ca2p and O1s increased gradually, while that of C1s decreased sharply, due to the chemical reaction between CaO and graphite-like phases and the coverage of RSB by CaO and $CaCO_3$. Moisture and CO_2 easily reacted with CaO to form $Ca(OH)_2$ and $CaCO_3$, respectively. CO_2 reacted with CaO and $Ca(OH)_2$ to form a thermodynamically stable $CaCO_3$. When the temperature rises, $CaCO_3$ undergo chemical reactions and are decomposed to form CaO (Wang et al., 2020a).

$$CaO_{(s)} + CO_2 \rightarrow CaCO_{3(s)};\ \Delta G^o = -31.07\ \text{kcal mol}^{-1} \quad (1)$$

$$CaO_{(s)} + H_2O \rightarrow Ca(OH)_{2(s)};\ \Delta G^o = -15.30\ \text{kcal mol}^{-1} \quad (2)$$

$$Ca(OH)_{2(s)} + CO_2 \rightarrow CaCO_{3(s)} + H_2O;\ \Delta G^o = -15.78\ \text{kcal mol}^{-1} \quad (3)$$

The results showed the presence of CaO and $CaCO_3$ in RSB900, along with low intensity peaks of carbon content, which suggested that RSB was carbonated with CO_2 and $CaCO_3$ was formed.

The calcium level increased from 50% (RSB300) to 65% (RSB900) with increasing temperature owing to the increase in CaO and $CaCO_3$ resulted from the pyrolysis process. The oxygen level decreased from 54% (RSB300) to 48% (RSB900) with increase in pyrolysis temperature due to the increase in oxygen-containing groups (OFGs), such as ketones and carbonyls introduced through surface modifications, which enhanced SPC activation in the carbocatalysis process (Yin et al., 2020). However, the carbon level decreased from 51% (RSB300) to 46% (RSB900) because of the decomposition of unstable C species.

Fig. 2e shows the LSV of RSB samples. Results showed that the current intensity followed the order: RSB300 < RSB500 < RSB700 < RSB900. RSB900 displayed the highest peak current among all RSB samples in the potential range of 0–2.0 V vs. Ag/AgCl, which was indicative of excellent electrical conductivity and favorable redox potential exhibited by the high-temperature pyrolyzed RSB compared with all other catalysts. In short, higher pyrolysis temperature resulted in higher graphitic degree and better conductivity, which facilitated electron transfer (Ho et al., 2019). As shown in Fig. 2f, the potential of RSB900 was −0.542 V vs. Ag/AgCl, more negative than that of RSB300 (−0.165 V vs. Ag/AgCl), which indicated that RSB900 underwent a higher corrosion rate in the presence of SPC, corresponding to faster electron transfer rate with lower corrosive potential (Zhou et al., 2020). According to previous studies, most of the biochar–based catalysts were prepared at relatively high temperature (≥700 °C), aimed to enhance the electrical conductivity (Minh et al., 2020). Overall, results implied that the intact sp^2-conjugated π structure as Lewis basic sites in RSB900 could donate e^- and facilitate electron transfer to SPC through the formation of more reactive oxygen species (ROS) than RSB300 by the following equation (Soltani et al., 2020):

$$RSB{-}\pi^+ + H_2O_2 \rightarrow RSB{-}\pi + HO\bullet + OH^- \quad (4)$$

3.2. Effect of SPC to DEHP degradation

DEHP was detected in the sediment samples at a concentration of 13,050 ± 1264 ng g^{-1} (or μg kg^{-1}) dry sediment. Based on sediment quality guideline (SQG) derived from biological effect data on aquatic organisms, the threshold effect level (TEL) and the probable effect level (PEL) of DEHP are 182 ng g^{-1} dw (dry weight) and 2647 ng g^{-1} dw, respectively (MacDonald et al., 1996). The DEHP concentration was 72 and 5 times that of TEL and PEL, respectively, in the sediments of Jen-Gen River. These data indicated that the sedimentary DEPH concentration might exhibit adverse impacts on benthic organisms. The results were consistent with those of previous studies (Chen et al., 2017), that DEHP was ubiquitous in the environment of the Jen-Gen River's estuary area in southern Taiwan. Furthermore, results of previous investigations indicated that the wide use of plasticizers might lead to increased levels of DEHP in the sediments (Zhang et al., 2018).

Fig. 3a shows the change of DEHP concentration as a function of reaction time as affected by the [DEHP] to [SPC] molar ratio. Results fitted well the pseudo-first-order kinetic model. Results indicated that high SPC dosage enhanced DEHP oxidation, though high SPC dosage implied increasing remediation costs. At the [DEHP] to [SPC] molar ratio of 1:1000, i.e., the highest SPC dosage, DEHP removal was 69%. Effective DEHP removal was attributable to the HO• generation from SPC. As shown in Fig. 3b, at [DEHP]/[SPC] ratio of 1:1000, the observed rate constant, k_{obs}, was $5.4 \times 10^{-2}\ h^{-1}$, almost 1.4 times that at [DEHP]/[SPC] ratio of 1:1. It has been reported that SPC is readily dissociated to CO_3^{2-} and H_2O_2. Under favorable pH, CO_3^{2-}, a Bronsted base, readily acquires a proton to become HCO_3^-. Catalytic decomposition of H_2O_2 yields HO• which reacts with carbonate/bicarbonate species (CO_3^{2-}/HCO_3^-) to form carbonate/bicarbonate radicals ($CO_3^{-\bullet}/HCO_3^{-\bullet}$) according to Eq. (5)–6 (Ma et al., 2018; Wang and Wang, 2019):

$$CO_3^{2-} + HO\bullet \rightarrow CO_3^{-\bullet} + OH^- \quad (5)$$

$$HCO_3^- + HO\bullet \rightarrow HCO_3^{-\bullet} + OH^- \quad (6)$$

Bicarbonate (HCO_3^-) and carbonate (CO_3^{2-}) are weak Bronsted acid/base which distribution is pH-dependent. Moreover, $CO_3^{-\bullet}$ could react with aromatic substrates via electron abstraction at a rate slower than HO• (Cui et al., 2017). Thus, $CO_3^{-\bullet}$ may play a pivotal role in the degradation of DEHP (Gao et al., 2020a). Based on

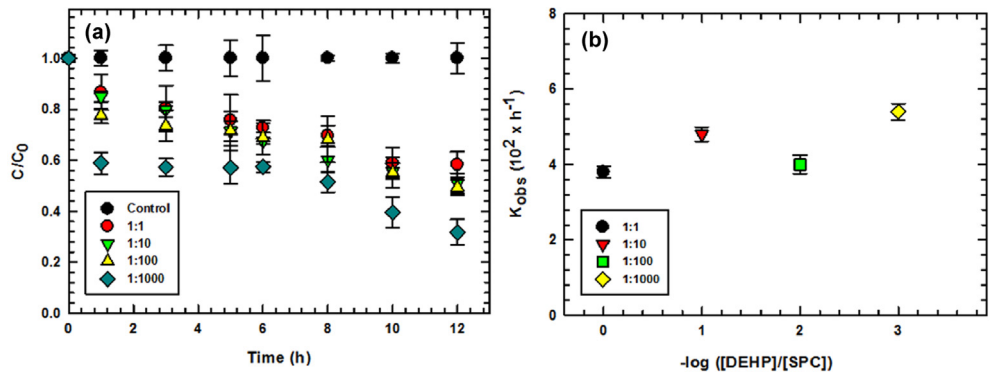

Fig. 3. (a) Change of DEHP concentration as a function of time as affected by percarbonate dosage; (b) observed DEHP degradation rate constant as a function of [DEHP] to [SPC] molar ratio. Experimental conditions: [sediment] = 2.5 g/L, temperature = 30 °C, initial pH = 9.0, control (solid dark circles); [DEHP]: [SPC] (molar ratio) = 1:1 ([DEHP] = [SPC] = 2×10^{-5} M) (solid red circles), = 1:10 ([DEHP] = 2×10^{-5} M; [SPC] = 2×10^{-4} M) (inverted green triangles), = 1:100 ([DEHP] = 2×10^{-5} M; [SPC] = 2×10^{-3} M) (yellow triangles), 1:1000 ([DEHP] = 2×10^{-5} M; [SPC] = 2×10^{-2} M) (dark green diamonds).

above results, SPC dosage of 2×10^{-4} M (or [DEHP]/[SPC] molar ratio of 1:10) was chosen as the optimal concentration for running more DEHP degradation experiments.

3.3. Effect of SPC over RSB catalyst on DEHP degradation

Additional experiments on the effect of pyrolysis temperature for RSB preparation and its impact on DEHP degradation by SPC. The result revealed that RSB900 was most effective in activating SPC to yield 63% of DEHP degradation, greater than 33% and 49% by RSB300 and SPC only, respectively. Carbocatalysis-driven SPC activation significantly enhanced DEHP degradation (Fig. 4a). Moreover, it could be concluded that the pyrolysis temperature played an important role on controlling the catalytic capacity of RSB. SPC was catalytically decomposed over RSB, rich in electron functionalities, thereby forming metastable complex. The complex aided in electron transfer on RSB via the intact sp^2-hybridized carbon π-network and converted the electrons into ROS, such as hydroxyl radicals (HO•). ROS in conjunction with $CaO/CaCO_3$ and RSB exhibited synergistic effects, which facilitated the catalytic redox reactions in the RSB900–SPC system and promoted the removal of DEHP (Wan et al., 2020).

High calcination temperature controlled the formation of graphitic carbon skeleton on biochar. Results of DEHP degradation as affected by the pyrolysis temperature agreed that of LSV characteristics (Fig. 2e). Yang et al. (2020) reported previously, that the sp^2/sp^3 configuration of carbon hybrids enabled carbocatalysts high catalytic activity toward SPC activation. Thus, RSB-based treatment by the reactive Ca-phases of contaminated sediments through SPC oxidation could be an economically appealing option in terms of cost savings in catalysts. The present study confirmed that RSB could effectively promote catalytic DEHP decomposition in estuarine sediments, specifically, by concurrently providing sufficient catalytic sites resulted from Ca^{2+} ion present abundantly for facilitating transfer of electrons on RSB. Marinković et al. (2016) reported the above similar observation that the basic surface CaO sites, which availability was controlled by its spatial dispersion, bringing about the catalytic activity. The basic sites reacted quickly with ambient H_2O and CO_2 to produce O^{2-} and initiated base-catalyzed reactions, which might be related to the relatively high contribution of CaO toward DEHP degradation. Furthermore, RSB/SPC also enhanced electron transfers and oxidative degradation of the DEHP via Ca^{2+}, through the initiation of oxidation-reduction reactions that generate ROS (Granados et al., 2007). The presence of OFGs (i.e., −OH and −COOH) on the RSB surface produced additional HO• that enhanced DEHP degradation further. In the present case, the aforementioned OFGs of the seaweed biomass facilitated adsorption/photocatalytic reactions of organic contaminants in the aqueous solution (Sharma et al., 2019).

The pseudo first order reaction kinetic expression described the oxidative degradation of DEHP well. The linear $\ln(C/C_0)$ vs. time (t) plot gave slope for the calculation of rate constant (k_{obs}), where C_0

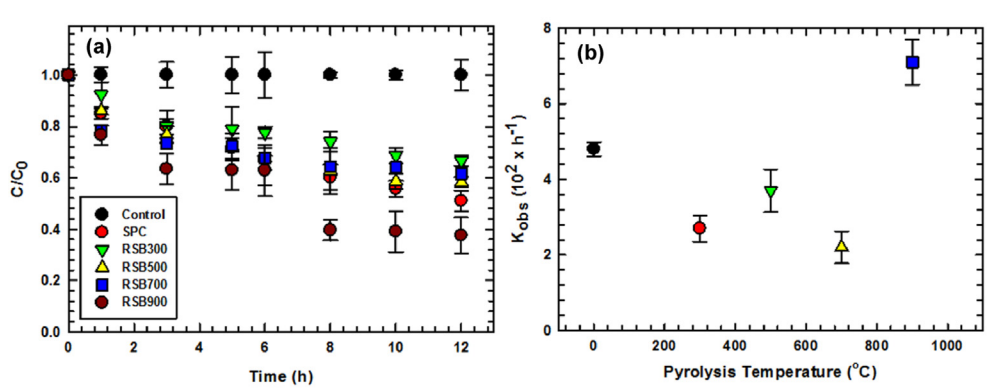

Fig. 4. (a) Change of DEHP concentration as a function of reaction time affected by the pyrolysis temperature for the preparation of RSB biochar; (b) observed DEHP degradation rate constant as a function of pyrolysis temperature. Experimental conditions: [sediment] = 2.5 g/L, temperature = 30 °C, initial pH = 9.0, [RSB] = 3.0 g/L, [SPC] = 2×10^{-4} M, [DEHP]: [SPC] (molar ratio) = 1 : 10.

and C are the DEHP concentration at the initial time (t = 0) and at time t, respectively (Fig. 4b). The k_{obs} value was 2.7×10^{-2}, 3.7×10^{-2}, 2.2×10^{-2}, and 7.1×10^{-2} h^{-1} for RSB300, RSB500, RSB700, and RSB900, respectively. RSB900 exhibited a 2.6-fold enhancement in the DEHP degradation rate over RSB300. Increase in the dipole moment of DEHP, due to changes in surface charge density on RSB upon positive or negative polarization, enhanced the π–π interactions between DEHP and RSB surface (Nie et al., 2019). Hence, the combined use of SPC and RSB for the degradation DEHP in the present study was rather innovative and genuinely promising.

The oxidation of DEHP in the RSB/SPC system was conducted at various RSB900 dosages (1.0–5.0 g L^{-1}) at constant total SPC concentration of 2×10^{-4} M and initial pH of 9.0. The addition of RSB at 3.0 g L^{-1} enhanced DEHP oxidation remarkably, due to generation of HO• in abundant quantity that achieved a maximum DEHP removal of 63% in 12 h. Results clearly indicated successful activation of SPC by RSB toward DEHP degradation (Fig. 5a). However, further increase in RSB dosage decreased DEHP degradation because of extensive SPC occupation of available active sites on the RSB surface. Additionally, excess SPC might be a quenching agent that consumed the generated ROS (Wu et al., 2020). Thus, the optimum DEHP degradation rate occurred at certain optimal RSB dose, e.g., 3 g/L.

Another hypothesis is that the reaction between HO• and hazardous organic compounds was reversible that oxidation between the organic chemicals in question with H_2O_2 occurred (Wang et al., 2019). Notably, some environmentally persistent free radicals (EPFRs), such as oxygen-, carbon-, and oxygenated carbon-centered radicals, were effectively activated by SPC in the presence of biochar and contributed to the enhanced removal of organic contaminants (Ruan et al., 2019). The above findings suggested that increasing direct electron transfers between the EPFRs on RSB surface, SPC (electron acceptor), and target contaminants (electron donor) in the electron-mediation regime enhanced the decomposition of DEHP in the RSB/SPC system because of increase in the production of HO• (Ho et al., 2019).

The observed DEHP degradation rate constant, k_{obs}, was 2.9×10^{-2}, 3.2×10^{-2}, 7.1×10^{-2}, 4.5×10^{-2}, and 1.8×10^{-2} h^{-1} at RSB dosage of 1.0, 2.0, 3.0, 4.0, and 5.0 g L^{-1}, respectively (Fig. 5b). Fig. 5b shows that the maximum k_{obs} occurred at an RSB dosage of 3.0 g L^{-1}, which was corresponded to the maximum DEHP degradation level. In summary, the increase in availability of SPC in solution and RSB surface resulted in the production of large amount of HO• removal which exhibited synergistic effects on DEHP removal in the RSB/SPC system.

The pH is a master variable of the aquatic system. It played a crucial role in sediment oxidative reactions. Fig. 6 gives results of DEHP removal as affected by initial pH (from 3.0 to 11.0) in the RSB/SPC system. It was noted that DEHP removal in alkaline solution was significantly greater than that in acidic or neutral medium. The DEHP degradation followed the order: pH 9.0 (63%) > pH 3.0 (45%) > pH 6.0 (44%) > pH 11.0 (27%) (Fig. 6a). Results indicated that an alkaline condition (pH 9.0) favored the production of abundant ROS from SPC and enhanced the degradation capacity than that of an acidic (pH 3.0) or neutral condition (pH 6.0). The degradation efficiency in pH 3.0 and pH 6.0 were similar, proving that the catalytic performance is efficient over a wide pH range. The similar effect was reported by Lai et al. (2019). However, because SPC was not effective at higher pH (e.g., 11.0) due to increase in ionic strength, which led to the less generation of HO• for DEHP degradation (Li et al., 2019). On the other hand, because SPC was not effectively being converted to CO_2 at alkaline pH, high pH (e.g., 11.0) inhibited the degradation of DEHP (Lyu et al., 2020). Therefore, the existing form of SPC acting as an oxidant is remarkably influenced by the solution pH. The dissociated SPC is relatively unstable and complex environmental conditions would further decrease its stability (Ma et al., 2020). Further studies will be conducted on the stability of the catalytic SPC degradation of DEHP in the presence of RSB at different pH values as to fully demonstrate the applicability of the RSB/SPC technology for the remediation of contaminated sediments. The dissociation of SPC produces Na^+, HCO_3^-, CO_3^{2-}, OH^-, and H_2O_2 (Eq. (7a)–b), which could initiated a series of reactions that formed several reactive species, e.g., $HO_2\bullet^-$, $HO\bullet^-$ and O_2 (Eq. (7c)–d). $CO_3^{-\bullet}$, possibly present in natural or slightly alkaline water systems, could potentially compete with organic contaminants for HO• radical. Studies have reported that $CO_3^{-\bullet}$ is more stable at near-neutral pH than in acidic condition (Cui et al., 2017). Because the initial solution pH in the RSB/SPC system was 9.0, therefore the amount of $CO_3^{-\bullet}$ would be rather small. Therefore, one could conclude that $CO_3^{-\bullet}$ might not influence DEHP degradation significantly. The results also suggested that HCO_3^- and CO_3^{2-} could activate SPC in a supplementary role, which further enhanced DEHP oxidation (Ma et al., 2018). The reaction between H_2O_2 and HCO_3^- led to the formation of $HCO_4^{\bullet-}$ (Eq. (7e)), which underwent hemolysis of the O–O bond to generate a series of active ROSs, including HO•, $HO_2\bullet^-$, $CO_3^{-\bullet}$, and $O_2^{-\bullet}$, according to the Eq. (7f)–k. These active species could also enhance the overall DEHP degradation capacity of the system (Eq. 7L).

$$2Na_2CO_3 \cdot 3H_2O_2 \rightarrow 2Na^+ + 2CO_3^{2-} + 3H_2O_2 \quad (7a)$$

$$CO_3^{2-} + H_2O \rightarrow HCO_3^- + OH^- \quad (7b)$$

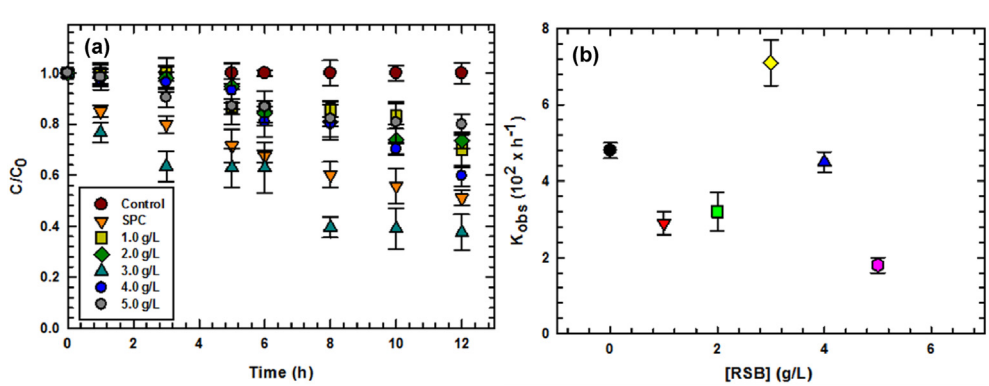

Fig. 5. (a) Change of DEHP concentration as a function of time affected by RSB dosage; (b) observed DEHP degradation rate constant as a function of RSB dosage. Experimental conditions: [sediment] = 2.5 g/L, temperature = 30 °C, initial pH = 9.0, [SPC] = 2×10^{-4} M, [DEHP]: [SPC] (molar ratio) = 1 : 10.

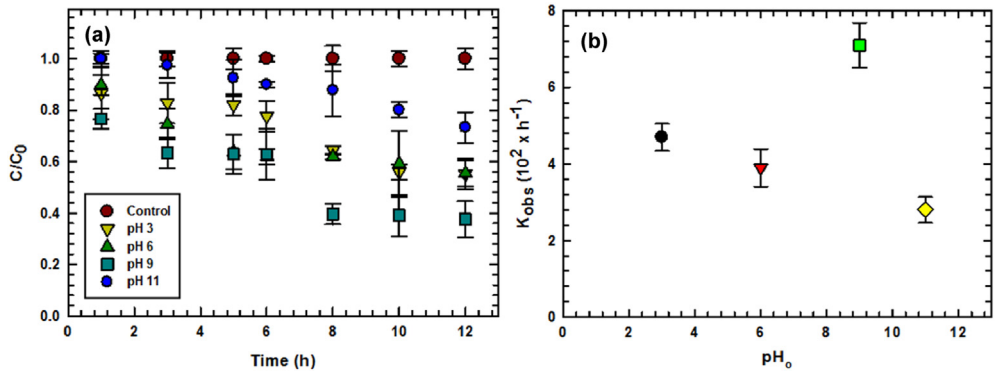

Fig. 6. (a) Change of DEHP concentration as a function of time affected by initial pH; (b) observed DEHP degradation rate constant as a function of initial pH. Experimental conditions: [sediment] = 2.5 g/L, temperature = 30 °C, [RSB] = 3.0 g/L, [SPC] = 2×10^{-4} M, [DEHP]: [SPC] (molar ratio) = 1 : 10.

$$H_2O_2 + OH^- \rightarrow HO_2\bullet^- + H_2O \quad (7c)$$

$$H_2O_2 + HO_2\bullet^- \rightarrow HO\bullet^- + O_2 + H_2O \quad (7d)$$

$$H_2O_2 + HCO_3^- \rightarrow HCO_4^{\bullet -} + H_2O \quad (7e)$$

$$HCO_4^{\bullet -} \rightarrow CO_3^{-\bullet} + HO\bullet \quad (7f)$$

$$H_2O_2 + CO_3^{-\bullet} \rightarrow HCO_3^- + HO_2\bullet^- \quad (7g)$$

$$HCO_3^- + HO\bullet \rightarrow CO_3^{-\bullet} + H_2O \quad (7h)$$

$$HO_2\bullet^- + HO\bullet \rightarrow O_2 + H_2O \quad (7i)$$

$$HO_2\bullet \rightarrow O_2^{-\bullet} + H^+ \quad (7j)$$

$$O_2^{-\bullet} + 2H_2O \rightarrow H_2O_2 + O_2 + H^+ \quad (7k)$$

$$DEHP + HO\bullet + O_2^{-\bullet} + O_2 \rightarrow \text{byproducts} + CO_2 + H_2O \quad (7l)$$

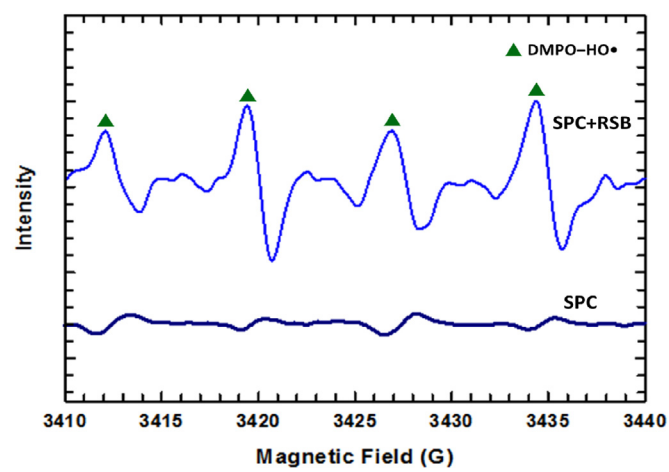

Fig. 7. Determination of reactive species by EPR in the RSB/SPC system.

The RSB activation of SPC produced sufficient HO• and $O_2^{-\bullet}$, which could carry out Fenton-like reaction by inducing electrophilic addition of HO• to aromatic rings and thus enhanced organic degradation (Fu et al., 2015), which again, explained why alkaline condition was more reactive than acidic condition toward DEHP removal. Our results were consistent with that of other reports on the degradation of organic compounds. However, a large number of CO_3^{2-} and HCO_3^- ions in the sediment would also compete with DEHP for ROSs, thereby hindering the degradation of DEHP (Lyu et al., 2020). Note that increase in pyrolysis temperature increased the ash content of the biochar, which subsequently increased the pH of seaweed biochar (Yu et al., 2017). Results suggested that significant degradation of DEHP occurred at the pH value in sediments because of the synergistic effects exhibited by RSB and HO•, the latter being the most active free radical for DEHP degradation reactions. The rate constant (k_{obs}), as affected by initial pH, of DEHP degradation followed the order: $k_{(pH\ 9.0)} > k_{(pH\ 3.0)} > k_{(pH\ 6.0)} > k_{(pH\ 11.0)}$ (Fig. 6b). EPR with DMPO in aqueous solution was carried out to verify the formation of free radicals species in the RSB/SPC system to determine the. The characteristic peaks of the DMPO-HO• adducts was observed, which suggested that HO• was the primary reactive ROS (Fig. 7), while $O_2^{-\bullet}$ might also contribute to the degradation of DEHP in the RSB/SPC system (Hung et al., 2020a). Results implied the vital role of $CaO/CaCO_3$ of RSB in enhancing efficient electron transfers between HO• and DEHP for efficient Fenton-like AOPs regarding radical generation. Results further demonstrated the importance of initial pH for DEHP degradation by SPC in the presence of RSB. The RSB/SPC system, at optimal operation conditions, significantly improved the degradation efficiency of DEHP in sediments over a wide pH range.

3.4. Microbial community

There is consensus that the abundance and diversity of a microbial community is directly related to ecological stability (Yamanaka et al., 2003; Panizzon et al., 2015). Results of Illumina MiSeq sequencing revealed the presence of 1245, 1258, 1329, and 1351 OTUs, respectively, in the original (control), SPC-, RSB-, and RSB/SPC- treated sediments. RSB/SPC treated sediments had the largest number of OTUs (Table 1). The average coverage of all samples was >99.5%. Compared to control, i.e., without any treatment, the addition of SPC and RSB enhanced the number of dominant bacteria, which was in accord with high DEHP removal efficiency. Moreover, the microbial diversity is closely related to the composition and activity of microorganisms and significantly impacts the fate of contaminants in DEHP-contaminated sediments (Gao et al., 2020b). To this end, the α-diversity index data were computed. Results showed no significant difference in OTU number, except the Simpson index, for the benthic bacteria in the RSB and SPC treated sediments. The Shannon index was greater than 5.0, which indicated high microbial diversity in the treated sediments. Noteworthy, a significantly higher Shannon index value was obtained in the RSB treated sediments than that of control, treated by SPC and RSB/SPC. Overall, RSB treatment increased the microbial

Table 1
Number of OTUs, species richness and diversity estimates of microbial communities indices based on the 16S rRNA gene after different treatment.

Treatment	OTUs	Simpson	Shannon	Chao01	ACE	Coverage
Sediment (Untreated sediment control)	1245	0.972	6.763	1436	1415	0.996
Sediment + SPC	1258	0.963	6.491	1466	1448	0.995
Sediment + RSB	1329	0.979	7.139	1460	1419	0.997
Sediment + RSB/SPC	1351	0.954	6.493	1664	1487	0.996

abundance in the sediment. DEHP contamination of the sediment could affect bacterial diversity and abundance. DEHP degradation increased the Chao1 and ACE indices, which implied high degree of microbial diversity and richness in the RSB/SPC treated sediments.

Changes in microbial distribution could have important ecological implications, particularly in sediment ecosystems (Chen et al., 2019). The distribution of core microbial community was uniform in all three sediment treatments (Fig. 8a). There were four major phyla (*Proteobacteria*, *Bacteroidetes*, *Synergistetes*, *Planctomycetes*) present in all sediment samples, with *Proteobacteria* being the main species as shown by the ternary plot analysis. Moreover, *Synergistetes* was enriched in the control sediment, *Actinobacteria* and *Chloroflexi* were enriched in the sediment treated by SPC, and *Epsilonbacteraeota* was enriched in the sediment treated by RSB/SPC. Our findings were supported by results reported by Du et al. (2020) and Cheema et al. (2015) who observed that *Actinobacteria* were catalase-positive microorganisms tolerable and capable of decomposing SPC as sole carbon and energy source in water, while *Chloroflexi* were the dominant phyla related to the degradation of petroleum pollutants. It has been reported that *Proteobacteria*, *Bacteroidetes*, and *Actinobacteria* play a central role in the mineralization of DEHP-contaminated soils (Zhu et al., 2019; Gao et al., 2020b). These three phyla accounted for 84% of the total bacteria population and constituted the main community members for the decomposition of pollutants. In order to compare the bacterial community composition in the four treated sediments, a Venn diagram was constructed as shown in Fig. 8b. A total of 854 OTUs overlapped among the control and three treated sediments. There were 90, 99, 102, and 142 unique OTUs for the control, SPC-, RSB-, and RSB/SPC- treated sediments, respectively. The data reflected the difference in community structure among the sediments of four treatments. Moreover, the RSB/SPC treated sediment exhibited the largest number of unique OTUs, which indicated that RSB/SPC treatment significantly promoted the microbial diversity of the sediment.

The distribution of the top 10 OTUs accounted for 97% of the bacteria population at the phylum level, as showed in Fig. 9a. Results indicated that *Bacteroidetes* and *Proteobacteria* (16.9 and 49.7%, respectively) were more abundant in the control than the other treated sediment samples. In addition, the phyla of *Actinobacteria* and *Thermotogae* (1.4 and 1.3%, respectively) also appeared as minor components in the sediments. Therefore, the sediments were dominated by *Proteobacteria* and *Bacteroidetes*. The sediment treated by SPC contained *Bacteroidetes* and *Proteobacteria*, at relative abundance of 15.7 and 51.4%, respectively, whereas *Synergistetes* was the third most relative abundant phylum. *Proteobacteria* had the highest relative abundance (43.9%) in the RSB treated sediment sample but was the smallest among sediments without being untreated and treated with SPC and RSB/SPC. In the RSB/SPC treated sediment sample, *Bacteroidetes* and *Proteobacteria* were the most abundant (15.6 and 54.5%) phyla except that the relative abundance of *Proteobacteria* was greater than that of the control and other sediment treated by SPC and RSB, separately. It is worthy of mentioning that adding biochar to sediments enriched the microbial population due to improvements in sediment permeability, water retention, and nutrient contents, which in turn enhanced the removal of organic contaminants (Wang and Wang, 2020). Moreover, decrease in DEHP concentration increased the abundance of the *Proteobacteria* phylum notably in the RSB/SPC treated sediment. Our result agreed with that of Wang et al. (2020b) who observed *Proteobacteria* and *Bacteroidetes* as the most abundant bacterial phyla during DEHP biodegradation in an activated sludge treatment system.

Fig. 9b shows that the top 10 OTUs accounted for 90% of the bacteria class in the sediments. *Synergistia*, *Planctomycetacia*, *Alphaproteobacteria*, *Bacteroidia*, and *Gammaproteobacteria* (7.0, 8.0, 11.8, 15.0, and 36.1%) were more abundant class in the control and the other three treated sediment samples, while *Anaerolineae* and *Rhodothermia* (1.3 and 1.6%) were less abundant class. *Alphaproteobacteria*, *Bacteroidia*, and *Gammaproteobacteria* had higher relative abundance (14.4, 14.8, and 35.9%, respectively) in the SPC treated sediment than the control sediment, whereas *Rhodothermia* was less abundant class. In the RSB treated sediment, *Gammaproteobacteria* had the highest relative abundance (30.6%) but was

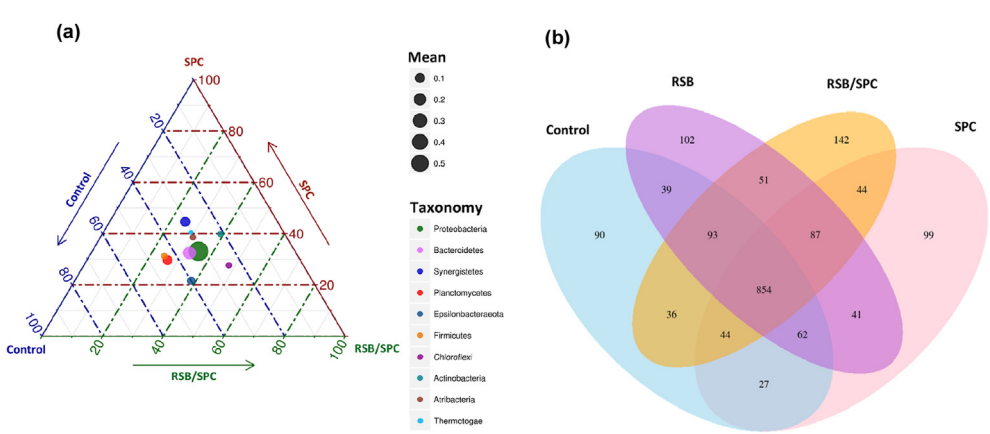

Fig. 8. (a) Ternary plot and (b) Venn diagram at the phylum level within different treatments and the control (sediment).

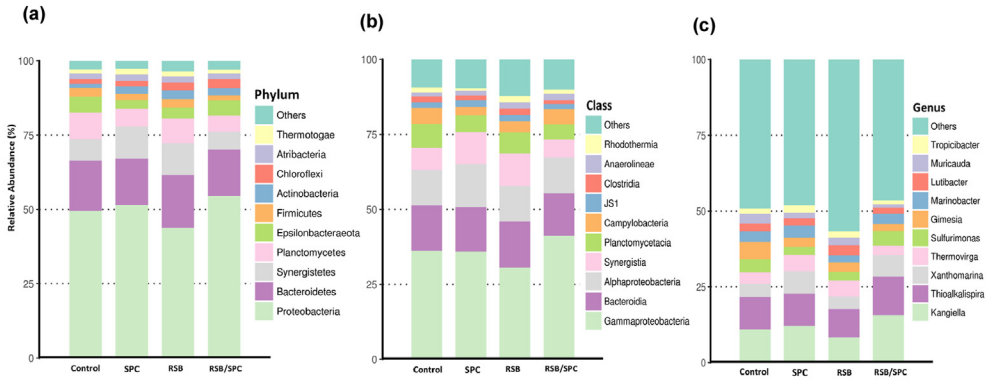

Fig. 9. Histogram of the relative abundance of the top 10 bacteria OTUs at the (a) phylum, (b) class, and (c) genus level in sediments received different treatments.

slightly smaller than the control and other treated sediments. In the RSB/SPC treated sediment, *Gammaproteobacteria*, was the most abundant class (41.2%) relative to the control and other treated sediment samples. Results of principal component analysis showed that the dominant *Gammaproteobacteria* class belong to the *Proteobacteria* phylum, which appeared to dominant the microbial community after treatment with SPC, RSB, and RSB/SPC. The above results suggested that changes at the class level were mainly determined by the DEHP degradation process, in which *Gammaproteobacteria* was the keystone class.

Fig. 9c shows the identified genus (accounting for 43–53%) include *Marinobacter*, *Thermovirga*, *Xanthomarina*, *Thioalkalispira*, and *Kangiella* (4.1, 5.3, 7.4, 10.7, and 10.9%, respectively), which were more abundant in the control than in the other three treated sediments, while *Tropicibacter* and *Lutibacter* (1.7 and 2.5%) were less abundant genus. *Xanthomarina*, *Thioalkalispira*, and *Kangiella* had a higher relative abundance (7.4, 10.6, and 12.1%, respectively) in the SPC treated sample compared to the control sediment, whereas *Muricauda* was less abundant genus. *Thioalkalispira* had the highest relative abundance (9.3%) in the RSB treated sediment sample, when compared to that of other sediment treatments, while *Tropicibacter* was a less abundant genera. *Thioalkalispira,* also belonged to the *Gammaproteobacteria* class and *Proteobacteria* phylum, were enriched in the RSB-addition sediments. Therefore, the microbial community changed accordingly in the sediment ecosystem upon RSB treatment. In the RSB/SPC treatment system, *Kangiella*, was the most abundant genus (15.6%) compared to the other treatments, whereas *Muricauda* was less abundant genus. Results of the principal component analysis showed that the dominant *Kangiella* genus belonged to the *Gammaproteobacteria* class and *Proteobacteria* phylum, which appeared to dominant after RSB/SPC treatment. Again, above results suggested that changes at the genus level were mainly determined by the DEHP degradation process, in which *Proteobacteria* was the keystone phylum. Liang et al. (2018) studied changes in the sediment microbial community in association with phthalate biodegradation and reported that aerobic *Proteobacteria* was predominated during phthalate degradation in sediments, which suggested that these bacteria were capable of utilizing DEHP as carbon and energy resource in the DEHP degradation process. Hence, the resistant bacteria have the potential to tolerate and degrade DEHP in contaminated sediments.

Based on the heatmap analysis, the SPC treated sediment contained *Thermovirga* and *Atribacteria* at higher relative abundances than the control treatment, whereas *Deinococcus_Thermus* was less abundant (Fig. 10a). *Dadabacteria*, *Fusobacteria*, *Acidobacteria*, *Latescibacteria*, *Dependentiae*, *WS2*, *Cyanobacteria*, *Bacteroidetes*, and *Gemmatimonadetes* exhibited the highest relative abundances in the RSB treated sediment, while *Proteobacteria* was less abundant. The results suggested that the above bacterial groups might be responsible for the degradation of DEHP in the sediment environment. Previously reported results demonstrated that *Gemmatimonadetes*, *Acidobacteria*, and *Bacteroidetes* were among the main DEHP decomposers under aerobic conditions (Zhu et al., 2020). *Patescibacteria*, *Spirochaetes*, and *Calditrichaeota* exhibited the highest relative abundance in the RSB/SPC treatment system, while *TA06* was less abundant. At the class level, the SPC treatment produced *Thermotogae*, *Alphaproteobacteria*, and *WCHB1_81*, which had higher relative abundance than the control treatment, whereas *Deltaproteobacteria* was less abundant (Fig. 10b). *Holophagae*, *Phycisphaerae*, *Chloroflexia*, *Babeliae*, and *Acidimicrobiia* exhibited the highest relative abundance in the RSB treatment system, while *Gammaproteobacteria* were less abundant. SPC treatment exhibited the highest relative abundance in *Thermotogae*, *Alphaproteobacteria*, and *WCHB1_81*, while *Deltaproteobacteria* was less abundant. The RSB/SPC treatment exhibited the highest relative abundance in *KD4_96*, *Coriobacteriia*, and *Spirochaetia*, while *Bacteroidia* was less abundant. Moreover, at the genus level, *Draconibacterium*, *Sneathiella*, *Gimesia*, and *Bacillus* were more abundant in the control sediment compared to the three treatment systems (Fig. 10c). It was previously suggested that *Bacillus* was critically responsible for PAE degradation (Priya and Jayachandran, 2012). Furthermore, the biodegradation rate of DEHP during the composting of mangrove sediment was significantly correlated to the abundance of *Bacillus* (Yuan et al., 2010). The SPC treatment system had higher relative abundance in *Verticia*, *Marinicella*, *Nitratireductor*, and *Mesotoga* than the control treatment, whereas *Sedimenticola* and *Gracilimonas* were less abundant. RSB treatment system exhibited the highest relative abundance in *Arenibacter*, *Vitellibacter*, *Rhodopirellula*, *SM1A02*, *Lutibacter*, and *ADurbBin120,* while *Thalassospira* and *Marinobacter* were less abundant. The dominant bacterial community changed drastically to *Thioalkalispira* and *Kangiella*, most of which belonged to the *Proteobacteria* phylum and *Gammaproteobacteria* class in the RSB/SPC treatment system. The results suggested that the bacteria, the phylum *Proteobacteria*, genus *Thioalkalispira*, and *Kangiella* in the original sediment could tolerate changes of environmental conditions during the remediation process. It was therefore concluded that, under the current experimental conditions, effectively increasing the abundance of bacterial communities via the addition of both RSB and SPC might be key to increasing the bioavailability of DEHP in the sediment treatment system. Thus, the RSB/SPC-based technology offers cost-effective and eco-friendly attractive strategy for the remediation of DEHP-contaminated sediments.

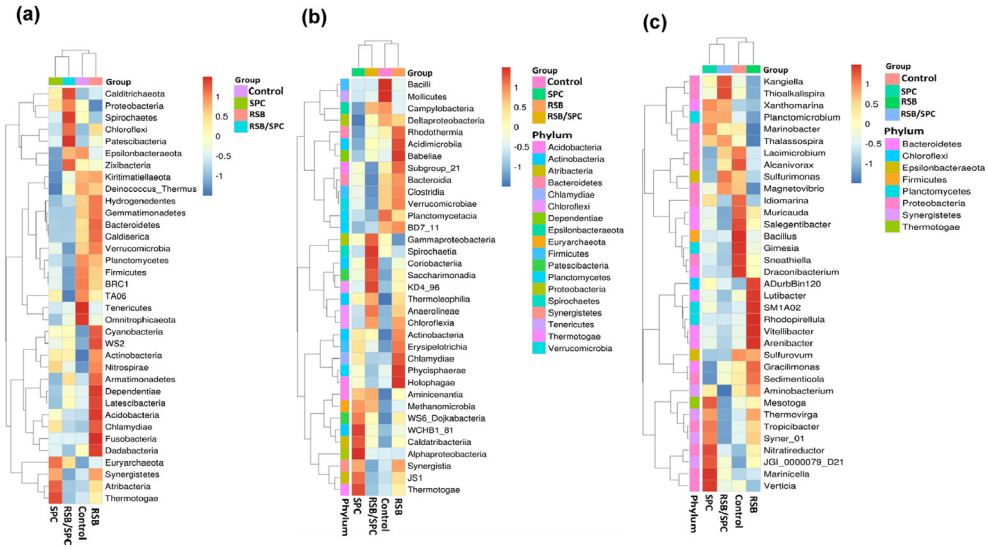

Fig. 10. z-score hierarchical clustering analysis and heatmaps of the relative abundance of the top 35 bacteria OTUs at the (a) phylum, (b) class, and (c) genus level in sediments received different treatments.

4. Conclusions

The effects of carbocatalysis and the addition of biochar, prepared from red seaweed residues, in tandem with SPC treatment of sediments contaminated with DEHP were studied. The changes in the bacteria community structure during DEHP degradation were also assessed. The results demonstrated that RSB activation of SPC directly generated HO•, which was major species responsible for DEHP oxidation. The unique structural configuration with the sp^2-hybridized carbon network on the surface of RSB nanoparticles contributed catalytically active sites for SPC activation. Meanwhile, the electron transfers during SPC activation also controlled the electronic property of RSB catalysts. Pseudo-first-order kinetics described the DEHP degradation well in the RSB/SPC system. Illumina MiSeq sequencing revealed that RSB/SPC treatment significantly affected the microbial community of the sediment. The results identified the microorganisms that were better tolerant to changes of environmental conditions during RSB/SPC treatment, thus offering an alternative to the *in-situ* bioremediation of DEHP-contaminated sediments. Overall, results demonstrated the effective treatment of DEHP-laden sediments by SPC and seaweed-derived materials, namely RSB, in an economical and eco-friendly manner, enabling a promising and sustainable circular bioeconomy.

CRediT authorship contribution statement

Chang-Mao Hung: Conceptualization, Methodology, Investigation, Validation, Formal analysis, Writing - original draft. **Chin-Pao Huang:** Writing - review & editing, Visualization. **Chiu-Wen Chen:** Resources. **Cheng-Di Dong:** Resources, Supervision.

Declaration of competing interest

The authors declare that they have no known competing financial interests or personal relationships that could have appeared to influence the work reported in this paper.

Acknowledgments

The authors would like to thank the Ministry of Science and Technology of Taiwan, for financial support to perform this study under Contract Nos. MOST 106-2221-E-022-002-MY3, 106-2221-E-022-003-MY3 and 108-2221-E-992-051-MY3. Addition support was provided by US NSF IOA (1632899) to CPH.

Appendix A. Supplementary data

Supplementary data to this article can be found online at https://doi.org/10.1016/j.jclepro.2021.126108.

References

Annamalai, J., Vasudevan, N., 2020. Enhanced biodegradation of an endocrine disruptingmicro-pollutant: di (2-ethylhexyl) phthalate using biogenic self-assembled monolayer of silver nanoparticles. Sci. Total Environ. 719, 137115.
Azargohar, R., Nanda, S., Dalai, A.K., Kozinski, J.A., 2019. Physico-chemistry of biochars produced through steam gasification and hydro-thermal gasification of canola hull and canola meal pellets. Biomass Bioenergy 120, 458–470.
Cheema, S., Lavania, M., Lal, B., 2015. Impact of petroleum hydrocarbon contamination on the indigenous soil microbial community. Ann. Microbiol. 65, 359–369.
Chen, C.F., Chen, C.W., Ju, Y.R., Dong, C.D., 2017. Determination and assessment of phthalate esters content in sediments from Kaohsiung Harbor, Taiwan. Mar. Pollut. Bull. 124, 767–774.
Chen, C.Y., Wu, P.S., Chung, Y.C., 2009. Coupled biological and photo-Fenton pretreatment system for the removal of di-(2-ethylhexyl) phthalate (DEHP) from water. Bioresour. Technol. 100, 4531–4534.
Chen, L., Xiang, W., Wu, H., Ouyang, S., Zhou, B., Zeng, Y., Chen, Y., Kuzyakov, Y., 2019. Tree species identity surpasses richness in affecting soil microbial richness and community composition in subtropical forests. Soil Biol. Biochem. 130, 113–121.
Chen, Y., Duan, X., Zhang, C., Wang, S., Ren, N., Ho, S.H., 2020. Graphitic biochar catalysts from anaerobic digestion sludge for nonradical degradation of micropollutants and disinfection. Chem. Eng. J. 384, 123244.
Cui, H., Gu, X., Lu, S., Fu, X., Zhang, X., Fu, G.Y., Qiu, Z., Sui, Q., 2017. Degradation of ethylbenzene in aqueous solution by sodium percarbonate activated with EDDS–Fe(III) complex. Chem. Eng. J. 309, 80–88.
De Bhowmick, G., Sarmah, A.K., Sen, R., 2018. Production and characterization of a value added biochar mix using seaweed, rice husk and pine sawdust: a parametric study. J. Clean. Prod. 200, 641–656.
Dong, C.D., Chen, C.W., Hung, C.M., 2017. Synthesis of magnetic biochar from bamboo biomass to activate persulfate for the removal of polycyclic aromatic hydrocarbons in marine sediments. Bioresour. Technol. 245, 188–195.
Dong, C.D., Chen, C.W., Kao, C.M., Chien, C.C., Hung, C.M., 2018. Wood-biochar-supported magnetite nanoparticles for remediation of PAH-contaminated estuary sediment. Catalysts 8, 73–86.
Dong, C.D., Chen, C.W., Hung, C.M., 2019a. Persulfate activation with rice-husk-based magnetic biochar for degrading PAEs in marine sediments. Environ. Sci. Pollut. Res. 26, 33781–33790.
Dong, C.D., Huang, C.P., Nguyen, T.B., Hsiung, C.F., Wu, C.H., Lin, Y.L., Chen, C.W., Hung, C.M., 2019b. The degradation of phthalate esters in marine sediments by persulfate over iron–cerium oxide catalyst. Sci. Total Environ. 696, 133973.

Dong, C.D., Chen, C.W., Nguyen, T.B., Huang, C.P., Hung, C.M., 2020a. Degradation of phthalate esters in marine sediments by persulfate over Fe–Ce/biochar composites. Chem. Eng. J. 384, 123301.
Dong, C.D., Tsai, M.L., Wang, T.H., Chang, J.H., Chen, C.W., Hung, C.M., 2020b. Removal of polycyclic aromatic hydrocarbon (PAH)-contaminated sediments by persulfate oxidation and determination of degradation product cytotoxicity based on HepG2 and ZF4 Cell Lines". Environ. Sci. Pollut. Res. 27, 34596–34605.
Du, Z., Jia, R., Li, C., Cui, P., Song, W., Liu, J., 2020. Pilot-scale UV/H_2O_2-BAC process for drinking water treatment – analysis and comparison of different activated carbon columns. Chem. Eng. J. 382, 123044.
Fu, X., Gu, X., Lu, S., Miao, Z., Xu, M., Zhang, X., Qiu, Z., Sui, Q., 2015. Benzene depletion by Fe^{2+}-catalyzed sodium percarbonate in aqueous solution. Chem. Eng. J. 267, 25–33.
Gao, D.W., Wen, Z.D., 2016. Phthalate esters in the environment: a critical review of their occurrence, biodegradation, and removal during wastewater treatment processes. Sci. Total Environ. 541, 986–1001.
Gao, J., Duan, X., O'Shea, K., Dionysiou, D.D., 2020a. Degradation and transformation of bisphenol A in UV/Sodium percarbonate: dual role of carbonate radical anion. Water Res. 171, 115394.
Gao, M., Zhang, Z., Dong, Y., Song, Z., Dai, H., 2020b. Responses of bacterial communities in wheat rhizospheres in different soils to di-n-butyl and di(2-ethylhexyl)phthalate contamination. Geoderma 362, 114126.
Gou, Y., Zhao, Q., Yang, S., Wang, H., Qiao, P., Song, Y., Cheng, Y., Li, P., 2020. Removal of polycyclic aromatic hydrocarbons (PAHs) and the response of indigenous bacteria in highly contaminated aged soil after persulfate oxidation. Ecotoxicol. Environ. Saf. 190, 110092.
Granados, M.L., Poves, M.D.Z., Alonso, D.M., Mariscal, R., Galisteo, F.C., Moreno-Tost, R., Santamaría, J., Fierro, J.L.G., 2007. Biodiesel from sunflower oil by using activated calcium oxide. Appl. Catal. B Environ. 73, 317–326.
Ho, S.H., Chen, Y.D., Li, R., Zhang, C., Ge, Y., Cao, G., Ma, M., Duan, X., Wang, S., Ren, N.Q., 2019. N-doped graphitic biochars from C-phycocyanin extracted Spirulina residue for catalytic persulfate activation toward nonradical disinfection and organic oxidation. Water Res. 159, 77–86.
Hu, H., Fang, S., Zhao, M., Jin, H., 2020. Occurrence of phthalic acid esters in sediment samples from East China Sea. Sci. Total Environ. 722, 137997.
Hung, C.M., Huang, C.P., Hsieh, S.L., Tsai, M.L., Chen, C.W., Dong, C.D., 2020a. Biochar derived from red algae for efficient remediation of 4-nonylphenol from marine sediments. Chemosphere 254, 126919.
Hung, C.M., Huang, C.P., Chen, C.W., Wu, C.H., Lin, Y.L., Dong, C.D., 2020b. Activation of percarbonate by water treatment sludge–derived biochar for the remediation of PAH-contaminated sediments. Environ. Pollut. 265, 114914.
Hung, C.M., Huang, C.P., Chen, S.K., Chen, C.W., Dong, C.D., 2020c. Electrochemical analysis of naproxen in water using poly(L-serine)-modified glassy carbon electrode. Chemosphere 254, 126686.
Hung, C.M., Huang, C.P., Lam, S.S., Chen, C.W., Dong, C.D., 2020d. The removal of polycyclic aromatic hydrocarbons (PAHs) from marine sediments using persulfate over a nano-sized iron composite of magnetite and carbon black activator. J. Environ. Chem. Eng. 8, 104440.
Hung, C.M., Huang, C.P., Chen, C.W., Hsieh, S.L., Dong, C.D., 2021. Effects of biochar on catalysis treatment of 4-nonylphenol in estuarine sediment and associated microbial community structure. Environ. Pollut. 268, 115673.
Lai, C., Huang, F., Zeng, G., Huang, D., Qin, L., Cheng, M., Zhang, C., Li, B., Yi, H., Liu, S., Li, L., Chen, L., 2019. Fabrication of novel magnetic $MnFe_2O_4$/bio-char composite and heterogeneous photo-Fenton degradation of tetracycline in near neutral pH. Chemosphere 224, 910–921.
Lam, S.S., Liew, R.K., Wong, Y.M., Azwar, E., Jusoh, A., Wahi, R., 2017. Activated carbon for catalyst support from microwave pyrolysis of orange peel. Waste Biomass Valorization 8, 2109–2119.
Li, L., Lai, C., Huang, F., Cheng, M., Zeng, G., Huang, D., Li, B., Liu, S., Zhang, M., Qin, L., Li, M., He, J., Zhang, Y., Chen, L., 2019. Degradation of naphthalene with magnetic bio-char activate hydrogen peroxide: synergism of bio-char and Fe–Mn binary oxides. Water Res. 160, 238–248.
Li, Y., Zhu, Y., Wang, D., Yang, G., Pan, L., Wang, Q., Ni, B.J., Li, H., Yuan, X., Jiang, L., Tang, W., 2020a. Fe(II) catalyzing sodium percarbonate facilitates the dewaterability of waste activated sludge: performance, mechanism, and implication. Water Res. 174, 115626.
Li, P., Cheng, X., Zhou, W., Luo, C., Tan, F., Ren, Z., Zheng, L., Zhu, X., Wu, D., 2020b. Application of sodium percarbonate activated with Fe(II) for mitigating ultrafiltration membrane fouling by natural organic matter in drinking water treatment. J. Clean. Prod. 269, 122228.
Liang, D.W., Zhang, T., Fang, H.H.P., He, J., 2008. Phthalates biodegradation in the environment. Appl. Microbiol. Biotechnol. 80, 183–198.
Liew, R.K., Azwar, E., Yek, P.N.Y., Lim, X.Y., Cheng, C.K., Ng, J.H., Jusoh, A., Lam, W.H., Ibrahim, M.D., Ma, N.L., Lam, S.S., 2018. Microwave pyrolysis with KOH/NaOH mixture activation: a new approach to produce micro-mesoporous activated carbon for textile dye adsorption. Bioresour. Technol. 266, 1–10.
Lyu, Y., Lyu, S., Tang, P., Jiang, W., Sun, Y., Li, M., Sui, Q., 2020. Degradation of trichloroethylene in aqueous solution by sodium percarbonate activated with Fe(II)-citric acid complex in the presence of surfactant Tween-80. Chemosphere 257, 127223.
Ma, J., Xia, X., Ma, Y., Luo, Y., Zhong, Y., 2018. Stability of dissolved percarbonate and its implications for groundwater remediation. Chemosphere 205, 41–44.
Ma, J., Yang, X., Jiang, X., Wen, J., Li, Y., Zhong, Y., Chi, L., Wang, Y., 2020. Percarbonate persistence under different water chemistry conditions. Chem. Eng. J. 389, 123422.
MacDonald, D.D., Carr, R.S., Calder, F.D., Long, E.R., Ingersoll, C.G., 1996. Development and evaluation of sediment quality guidelines for Florida coastal waters. Ecotoxicology 5, 253–278.
Marinković, D.M., Stanković, M.V., Veličković, A.V., Avramović, J.M., Miladinović, M.R., Stamenković, O.O., Veljković, V.B., 2016. Calcium oxide as a promising heterogeneous catalyst for biodiesel production: current state and perspectives. Renew. Sustain. Energy Rev. 56, 1387–1408.
Mi, L., Xie, Z., Zhao, Z., Zhong, M., Mi, W., Ebinghaus, R., Tang, J., 2019. Occurrence and spatial distribution of phthalate esters in sediments of the Bohai and Yellow seas. Sci. Total Environ. 653, 792–800.
Nie, C., Dai, Z., Meng, H., Duan, X., Qin, Y., Zhou, Y., Ao, Z., Wang, S., An, T., 2019. Peroxydisulfate activation by positively polarized carbocatalyst for enhanced removal of aqueous organic pollutants. Water Res. 166, 115043.
Panizzon, J.P., Junior, H.L.P., Knaak, N., Ramos, R.S., Zeigler, D.R., Fiuza, L.M., 2015. Microbial diversity: relevance and relationship between environmental conservation and human health. Braz. Arch. Biol. Technol. 58, 137–145.
Priya, A.M., Jayachandran, S., 2012. Induction of apoptosis and cell cycle arrest by Bis (2-ethylhexyl) phthalate produced by marine Bacillus pumilus MB 40. Chem. Biol. Interact. 195, 133–143.
Ren, Z., Cheng, X., Li, P., Luo, C., Tan, F., Zhou, W., Liu, W., Zheng, L., Wu, D., 2020. Ferrous-activated sodium percarbonate pre-oxidation for membrane fouling control during ultrafiltration of algae-laden water. Sci. Total Environ. 739, 140030.
Ruan, X., Sun, Y., Du, W., Tang, Y., Liu, Q., Zhang, Z., Doherty, W., Frost, R.L., Qian, G., Tsang, D.C.W., 2019. Formation, characteristics, and applications of environmentally persistent free radicals in biochars: a review. Bioresour. Technol. 281, 457–468.
Sharma, G., Bhogal, S., Gupta, V.K., Agarwal, S., Kumar, A., Pathania, D., Mola, G.T., Stadler, F.J., 2019. Algal biochar reinforced trimetallic nanocomposite as adsorptional/photocatalyst for remediation of malachite green from aqueous medium. J. Mol. Liq. 275, 499–509.
Soltani, R.D.C., Mahmoudi, M., Boczkaj, G., Khataee, A., 2020. Activation of peroxymonosulfate using carbon black nano-spheres/calcium alginate hydrogel matrix for degradation of acetaminophen: Fe_3O_4 co-immobilization and microbial community response. J. Ind. Eng. Chem. 91, 240–251.
USEPA, 2007. Phthalates. TEACH Chemical Summary Environmental Protection Agency, Washington DC.
Wan, Z., Sun, T., Tsang, D.C.W., Xu, Z., Khan, E., Liu, S.H., Cao, X., 2020. Sustainable impact of tartaric acid as electron shuttle on hierarchical iron-incorporated biochar. Chem. Eng. J. 395, 125138.
Wang, J., Wang, S., 2019. Reactive species in advanced oxidation processes: formation, identification and reaction mechanism. Chem. Eng. J. 401, 126158.
Wang, J., Wang, S., 2020. Preparation, modification and environmental application of biochar: a review. J. Clean. Prod. 227, 1002–1022.
Wang, Q., Zhang, X., Sun, S., Wang, Z., Cui, D., 2020a. Effect of CaO on pyrolysis products and reaction mechanisms of a corn stover. ACS Omega 5, 10276–10287.
Wang, Q., Jiang, L., Fang, C., Chen, L., 2020b. Effects of di-n-butyl phthalate and di-2-ethylhexyl phthalate on pollutant removal and microbial community during wastewater treatment. Ecotoxicol. Environ. Saf. 198, 1106652.
Wang, R.Z., Huang, D.L., Liu, Y.G., Zhang, C., Lai, C., Wang, X., Zeng, G.M., Gong, X.M., Duan, A., Zhang, Q., Xu, P., 2019. Recent advances in biochar-based catalysts: properties, applications and mechanisms for pollution remediation. Chem. Eng. J. 371, 380–403.
Wu, S., Liu, H., Yang, C., Li, X., Lin, Y., Yin, K., Sun, J., Teng, Q., Du, C., Zhong, Y., 2020. High-performance porous carbon catalysts doped by iron and nitrogen for degradation of bisphenol F via peroxymonosulfate activation. Chem. Eng. J. 392, 123683.
Xie, Y., Liu, H., Li, H., Tang, H., Peng, H., Zu, H., 2020. High-effectively degrade the di-(2-ethylhexyl) phthalate via biochemical system: resistant bacterial flora and persulfate oxidation activated by BC@Fe_3O_4. Environ. Pollut. 262, 114100.
Xu, J., Lu, Q., de Toledo, R.A., Shim, H., 2017. Degradation of di-2-ethylhexyl phthalate (DEHP) by an indigenous isolate Acinetobacter sp. SN13. Int. Biodeterior. Biodegradation. 117, 205–214.
Yamanaka, T., Helgeland, L., Farstad, I.N., Fukushima, H., Midtvedt, T., Brandtzaeg, P., 2003. Microbial colonization drives lymphocyte accumulation and differentiation in the follicle-associated epithelium of Peyer's patches. J. Immunol. 170, 816–822.
Yang, G., Wang, Z., Xian, Q., Shen, F., Sun, C., Zhang, Y., Wu, J., 2015. Effects of pyrolysis temperature on the physicochemical properties of biochar derived from vermicompost and its potential use as an environmental amendment. RSC Adv. 5, 40117.
Yang, Q., Chen, Y., Duan, X., Zhou, S., Niu, Y., Sun, H., Zhi, L., Wang, S., 2020. Unzipping carbon nanotubes to nanoribbons for revealing the mechanism of nonradical oxidation by carbocatalysis. Appl. Catal. B Environ. 276, 119146.
Yek, P.N.Y., Peng, W., Wong, C.C., Liew, R.K., Ho, Y.L., Mahari, W.A.W., Azwar, E., Yuan, T.Q., Tabatabaei, M., Aghbashlo, M., Sonne, C., Lam, S.S., 2020. Engineered biochar via microwave CO_2 and steam pyrolysis to treat carcinogenic Congo red dye. J. Hazard Mater. 395, 122636.
Yin, H., Guo, Q., Lei, C., Chen, W., Huang, B., 2020. Electrochemical-driven carbocatalysis as highly efficient advanced oxidation processes for simultaneous removal of humic acid and Cr(VI). Chem. Eng. J. 396, 125156.
Yu, J., Zhu, Z., Zhang, H., Shen, X., Qiu, Y., Yin, D., Wang, S., 2020. Persistent free radicals on N-doped hydrochar for degradation of endocrine disrupting compounds. Chem. Eng. J. 398, 125538.

Yu, K.L., Lau, B.F., Show, P.L., Ong, H.C., Ling, T.C., Chen, W.H., Ng, E.P., Chang, J.S., 2017. Recent developments on algal biochar production and characterization. Bioresour. Technol. 246, 2–11.
Yu, K.L., Chen, W.H., Sheen, H.K., Chang, J.S., Lin, C.S., Ong, H.C., Show, P.L., Ng, E.P., Ling, T.C., 2020. Production of microalgal biochar and reducing sugar using wet torrefaction with microwave-assisted heating and acid hydrolysis pretreatment. Renew. Energy 156, 349–360.
Yuan, S.Y., Huang, I.C., Chang, B.V., 2010. Biodegradation of dibutyl phthalate and di-(2-ethylhexyl) phthalate and microbial community changes in mangrove sediment. J. Hazard Mater. 184, 826–831.
Zhang, Z.M., Zhang, H.H., Zhang, J., Wang, Q.W., Yang, G.P., 2018. Occurrence, distribution, and ecological risks of phthalate esters in the seawater and sediment of Changjiang River Estuary and its adjacent area. Sci. Total Environ. 619–620, 93–102.
Zhao, H.M., Du, H., Lin, J., Chen, X.B., Li, Y.W., Li, H., Cai, Q.Y., Mo, C.H., Qin, H.M., Wong, M.H., 2016. Complete degradation of the endocrine disruptor di-(2-ethylhexyl) phthalate by a novel Agromyces sp. MT-O strain and its application to bioremediation of contaminated soil. Sci. Total Environ. 562, 170–178.
Zhou, M., Zhang, C., Yuan, Y., Mao, X., Li, Y., Wang, N., Wang, S., Wang, X., 2020. Pinewood outperformed bamboo as feedstock to prepare biochar-supported zero-valent iron for Cr^{6+} reduction. Environ. Res. 187, 109695.
Zhu, F., Zhu, C., Zhou, D., Gao, J., 2019. Fate of di (2-ethylhexyl) phthalate and its impact on soil bacterial community under aerobic and anaerobic conditions. Chemosphere 216, 84–93.
Zhu, F., Doyle, E., Zhu, C., Zhou, D., Gu, C., Gao, J., 2020. Metagenomic analysis exploring microbial assemblages and functional genes potentially involved in di (2-ethylhexyl) phthalate degradation in soil. Sci. Total Environ. 715, 137037.
Zubkova, V., Strojwas, A., Bielecki, M., Kieush, L., Koverya, A., 2019. Comparative study of pyrolytic behavior of the biomass wastes originating in the Ukraine and potential application of such biomass. Part 1. Analysis of the course of pyrolysis process and the composition of formed products. Fuel 254, 115688.
Zuo, S., Li, D., Xu, H., Xia, D., 2020. An integrated microwave-ultraviolet catalysis process of four peroxides for wastewater treatment: free radical generation rate and mechanism. Chem. Eng. J. 380, 122434.